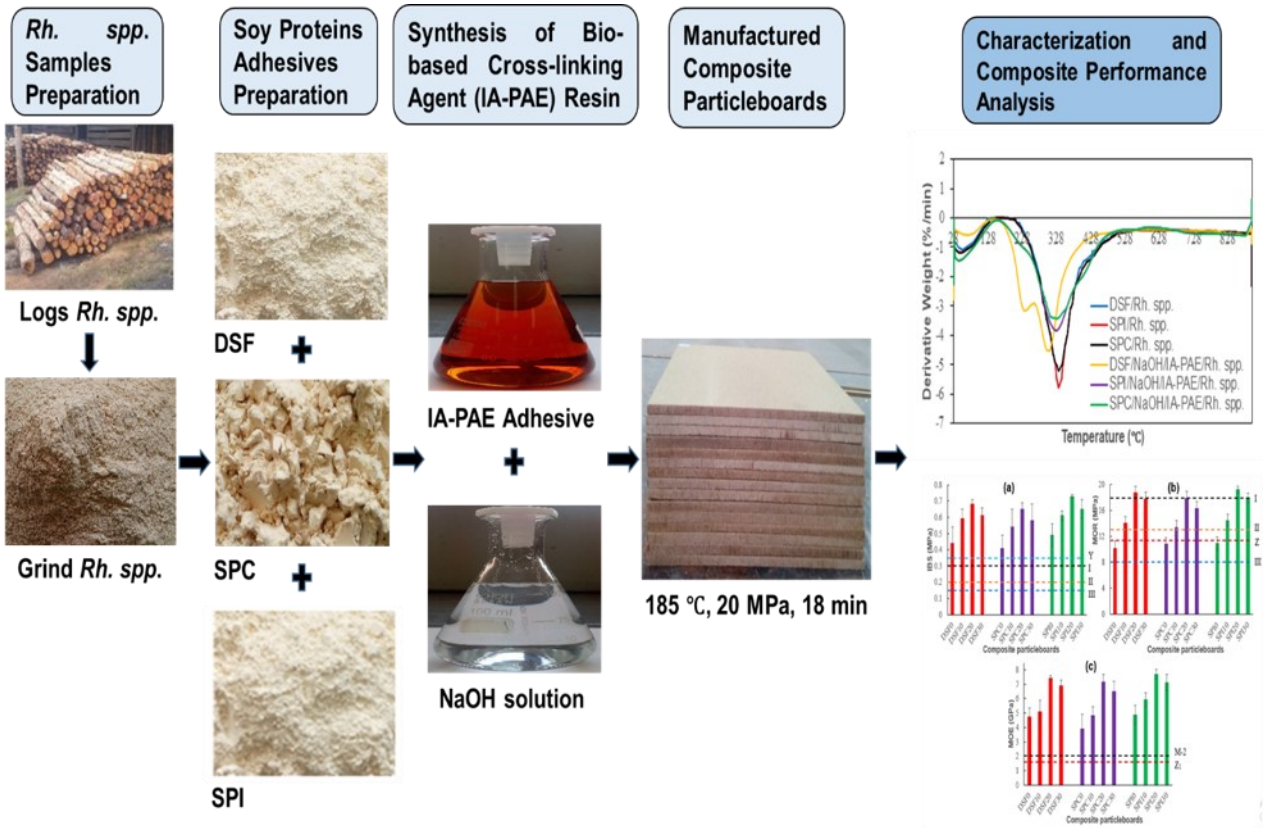
Sodium Hydroxide/Itaconic Acid Polyamidoamine-Epichlorohydrin Cross-linked Soy Protein Bonded *Rhizophora* spp. Composites

Damilola Oluwafemi Samson,[a,b] Siti Hajar Zuber ,[a,*] Saadiatul Nur Aqilah Mohd Zakaria,[a] Muhammad Safwan Ahmad Fadzil,[a] Abel Blessing Olorunsola,[b] Mohd Zahri Abdul Aziz,[c] Seán B. Leen,[d] and Pouyan Ghabezi [d]

* *Corresponding author: hajarzuber@ukm.edu.my*

DOI: 10.15376/biores.21.3.7769-7789

GRAPHICAL ABSTRACT



Sodium Hydroxide/Itaconic Acid Polyamidoamine-Epichlorohydrin Cross-linked Soy Protein Bonded *Rhizophora* spp. Composites

Damilola Oluwafemi Samson,[a,b] Siti Hajar Zuber ,[a,*] Saadiatul Nur Aqilah Mohd Zakaria,[a] Muhammad Safwan Ahmad Fadzil,[a] Abel Blessing Olorunsola,[b] Mohd Zahri Abdul Aziz,[c] Seán B. Leen,[d] and Pouyan Ghabezi [d]

Structural, thermal, and physicochemical performance were studied for sodium hydroxide (NaOH) (12 wt%)/itaconic acid polyamidoamine-epichlorohydrin (IA-PAE) (0 to 30 wt%) cross-linked tissue-equivalent composites made from defatted soy flour, soy protein concentrate, and soy protein isolate-bonded *Rhizophora* spp. (particle size: 149 µm), to enhance interfacial bonding, stability, and overall material performance. The Fourier transform infrared spectra confirmed effective crosslinking and a reduction in hydroxyl groups, with the formation of ester/ether linkages. Thermal analysis showed improved stability and a higher char yield. Microstructural analysis revealed denser, more homogeneous matrices with enhanced interfacial bonding. Average densities ranged (0.94 ± 0.11 to 1.04 ± 0.20 g/cm^3), matched those of water and other commercial tissue substitute biomaterials, while moisture content (6.51 ± 0.19 to 8.06 ± 0.50%) was consistent with JIS A-5908 (2015) limits. Mechanical properties exceeded standards (internal bonding strength (IBS) up to 0.73 ± 0.01 MPa; modulus of rupture (MOR): 19.21 ± 0.50 MPa; modulus of elasticity (MOE): 7.70 ± 0.33 GPa), and dimensional stability improved significantly (water absorption: ≥ 20%, thickness swelling: ≥ 10%). Optimal performance was achieved at 20% IA-PAE. NaOH/IA-PAE crosslinking effectively enhances structural, thermal, and physicomechanical properties, producing sustainable composite particleboards suitable for tissue-equivalent and radiation-related applications.

DOI: 10.15376/biores.21.3.7769-7789

Keywords: Soy protein-based adhesives; Rhizophora spp.; NaOH/IA-PAE crosslinking; Composite particleboards; Sustainable biomaterials; Renewable resources

Contact information: a: Department of Diagnostic Imaging and Radiotherapy, Centre of Diagnostic, Therapeutic and Investigate Studies, Faculty of Health Sciences, Universiti Kebangsaan Malaysia, 50300, Kuala Lumpur, Malaysia; b: Department of Physics, Faculty of Sciences, University of Abuja, 90021, Abuja, Nigeria; c: Biomedical Imaging Department, Pusat Kanser Tun Abdullah Ahmad Badawi, Universiti Sains Malaysia, Bertam, 13200, Kepala Batas, Pulau Pinang, Malaysia; d: School of Engineering, University of Galway, H91 TK33, Galway, Ireland;
** Corresponding author: hajarzuber@ukm.edu.my*

INTRODUCTION

Mangrove wood from the genus *Rhizophora* spp. (*Rh.* spp.) has attracted increasing interest as a sustainable raw material for engineered wood products, including particleboard, fiberboard, and plywood. Its fast growth, high density, and favorable mechanical strength make it particularly suitable for composite applications (Shakhreet *et*

al. 2013; Samson *et al.* 2020; Zuber *et al*. 2022). Beyond structural benefits, the unique anatomical features of *Rh.* spp., such as its stilt-like root system, enhance nutrient transport and environmental resilience, further supporting its use in advanced material systems (Ng *et al.* 1999). In addition to traditional applications, *Rh.* spp.-based materials have been investigated for radiation-related uses, including photon and electron radiotherapy, as well as X-ray attenuation, because of their promising shielding properties and tissue substitute performance (Banjade *et al.* 2001; Watanabe and Constantinou 2006; Abuarra *et al.* 2014; Hamid *et al.* 2018; Anugrah *et al.* 2020; Zuber *et al.* 2022; Samson *et al.* 2023; Tayo *et al.* 2025).

Despite these benefits, untreated *Rh.* spp. wood is susceptible to dimensional changes, biological decay, and mechanical wear over time. To address these problems, recent advances in wood-based composites have integrated wood adhesive systems to improve bonding performance and long-term stability (Abuarra *et al.* 2014; Samson *et al.* 2023; Zuber *et al.* 2025). Currently, approximately 95% of wood adhesive systems used worldwide to develop wood composites are based on non-renewable resources (synthetic adhesives) (Karliati *et al.* 2024). Conventional fossil-based adhesives, such as urea-formaldehyde, melamine-urea-formaldehyde, and phenol-formaldehyde resins, are widely used, with urea-formaldehyde particularly prevalent in the manufacturing of composite particleboards. While non-renewable resources offer strong bonding, improved efficiency, and performance, their environmental and health risks, such as formaldehyde emissions, coupled with their unsustainable nature, have fueled the search for cleaner alternative adhesives (Samson *et al.* 2020; Karliati *et al.* 2024; Xu *et al.* 2024; Tayo *et al.* 2025). Thermoplastic alternatives are more flexible but lack permanent cross-links, leading to reduced thermal and structural stability (Rowell *et al.* 2013; Marta *et al.* 2026).

In this context, bio-based adhesives made from renewable resources have become sustainable options because their by-products have resulted in optimized, economically feasible, and environmentally friendly value chains (Gui *et al.* 2013; Frihart and Satori 2013; Samson *et al.* 2025; Tayo *et al*. 2025; Marta *et al.* 2026; Younesi-Kordkheili and Pizzi 2026). Through reshaping linear industrial value chains to minimize pollution and waste generation, this shift supports a trajectory marked by greater sustainability and inclusivity, effectively addressing climate change and reducing reliance on fossil-based raw materials. Many renewable resources, including soy protein, tannins, corn starch, lignin, and animal glue, have so far been explored as alternatives for developing bio-adhesives (Abuarra *et al.* 2014; Xu *et al.* 2024; Samson *et al.* 2025; Tayo *et al.* 2025; Baskaran *et al.* 2026; Marta *et al.* 2026).

Among these biopolymers, soy protein-based adhesives (such as DSF-defatted soy flour, SPC-soy protein concentrate, and SPI-soy protein isolate) have been the most abundant oilseed-derived materials and have gained significant attention due to their biodegradability, availability, and excellent film-forming properties, as well as their use in tissue regeneration (Chien and Shah 2012; Xu *et al.* 2024; Samson *et al.* 2025). Soy proteins have complex hierarchical structures (α-helices and β-sheets) that influence their physicochemical behavior and adhesion capabilities. However, inherent limitations, including hydrophilicity, low water resistance, and moderate mechanical strength, restrict their use in high-performance composites (Hemmilä *et al.* 2017). To overcome these challenges, chemical modification and cross-linking are employed (Gui *et al.* 2013; Samson *et al.* 2020). Alkaline treatment with sodium hydroxide (NaOH) promotes protein unfolding and reactivity, while cross-linking agents, such as itaconic acid polyamidoamine-epichlorohydrin (IA-PAE), improve network formation, leading to

enhanced mechanical strength, water resistance, and interfacial bonding (Gui *et al.* 2013; Gao *et al.* 2019; Samson *et al.* 2020). These modifications are also expected to affect radiation attenuation by altering the composite's density and elemental composition.

This study focused on developing and characterizing *Rh.* spp.-based particleboards bonded with soy protein adhesives (DSF, SPC, and SPI) modified with NaOH (12 wt%) and varying levels of IA-PAE (0 to 30 wt%). The physicochemical, mechanical, and dimensional stability properties were evaluated, along with elemental atomic compositions. The performance of the composites was assessed in accordance with relevant standards, including the Japanese Industrial Standard (JIS A 5908 2015), the American Society for Testing and Materials (ASTM D1037 1999), and European standards (EN 319/EN 310 1993).

EXPERIMENTAL

Preparation and Particle Size Analysis of *Rhizophora* spp. Wood

Due to the natural variability in *Rh.* spp. wood from the local mangrove forest reserve in Perak, Malaysia, the middle trunk sections were selected. The debarked logs were cleaned, oven-dried, and cut into smaller pieces with a band saw, then planed into chips (~8370 µm). The chips were pre-ground (~1500 µm) with a mechanical grinder (3 krpm) and further milled to ≤ 500 µm using an SK-100 cutting mill (Retsch, Germany).

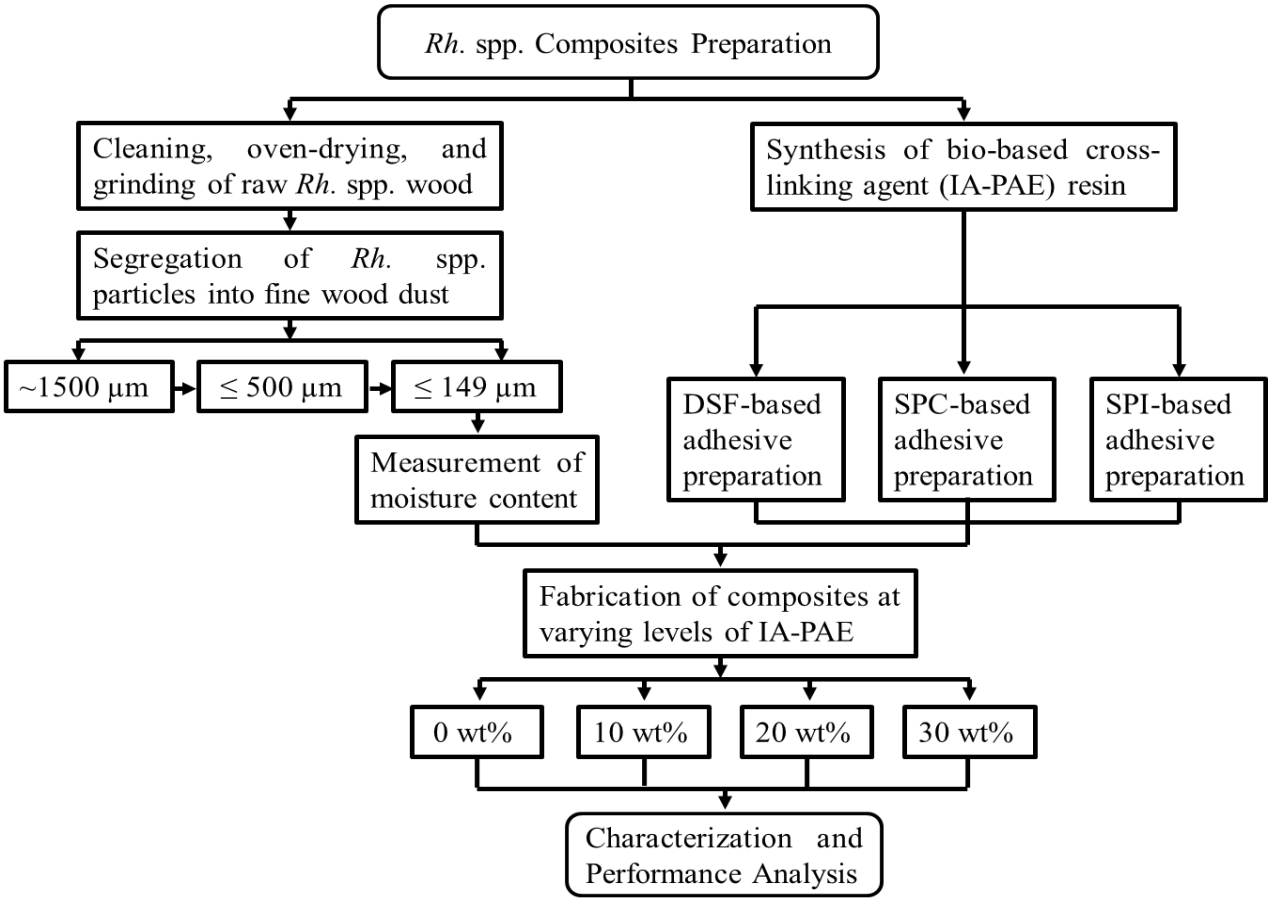


Fig. 1. Flowchart of the production process of bio-based *Rh.* spp. composites

The resulting particles (moisture content: 5 to 8%) were sieved (≤ 149 µm mesh) for 60 min using an automatic horizontal vibrating sieve (Tai-Yi, Taiwan), then conditioned at room temperature for 1 h and stored in sealed containers at ambient conditions for one month. *Rh*. spp. particles (≤ 149 µm) were used, as this size was previously identified as optimal for improving the physical and mechanical properties of the composites (Samson *et al.* 2020, 2023). Figure 1 illustrates the overall flowchart of the present study.

Preparation of NaOH/IA-PAE-modified Bio-Adhesives

The DSF, SPC, and SPI-based adhesives were purchased from Wachsen Industry and Shandong Wonderful Biotech (Qingdao, China) and supplied as mechanically pulverized, dehydrated powders (DSF: ≥ 50% w/w gross protein on a dry basis, ≤ 40% carbohydrates, ≤ 5.3% moisture, ≤ 6.5% ash, ≤ 1% crude fat; SPC: ≥ 65% w/w gross protein on a dry basis, ≤ 35% carbohydrates, ≤ 5.7% moisture, ≤ 8% ash, ≤ 0% crude fat; SPI: ≥ 90% w/w gross protein on a dry basis, ≤ 10% carbohydrates, ≤ 5% moisture, ≤ 6% ash, ≤ 0% crude fat). NaOH (≥ 97% purity) was obtained from Sigma-Aldrich (USA). The IA-PAE cross-linker was prepared according to established procedures reported in the literature (Samson *et al.* 2020).

DSF-, SPC-, and SPI-based/NaOH/IA-PAE adhesives were prepared following the method reported by Samson *et al.* (2020) with some modifications. For DSF-SPC systems, 35 g (dry basis) was dispersed in distilled water (65, 43, 33, and 23 g, corresponding to different solid contents) and mechanically stirred at 600 rpm for 30 min at 25 °C. IA-PAE resin (0, 10, 20, and 30 wt%, based on protein weight) was then added, and mechanical stirring was continued for an additional 30 min. For SPI formulations, 18 g of SPI was dissolved in distilled water (82, 60, 50, and 40 g), and mechanically stirred at 600 rpm for 30 min at 25 °C. IA-PAE (0 to 30 wt%, based on SPI weight) was subsequently added dropwise, followed by further mechanical stirring for 30 min. In all cases, the adhesive slurries were adjusted to pH 11.0 using 2 M NaOH (12 wt%), *via* dropwise addition over 30 min, and further mechanically mixed for 30 min to ensure homogeneity. The resulting formulations were designated as DSF-SPC-SPI/NaOH/IA-PAE adhesives. The composite variants were defined solely by protein type (DSF, SPC, or SPI) and IA-PAE content (0, 10, 20, and 30 wt%). A total of twelve adhesive formulations were prepared and evaluated.

Preparation of NaOH/IA-PAE-modified Composite Particleboards

Rh. spp. particles were uniformly blended with the respective adhesive formulations (DSF-, SPC-, or SPI-based + NaOH + IA-PAE) using a rotary mixer (DFY-1000, China) at 25 rpm for 40 min before composite fabrication. The mixtures were then formed into composite mats using a square mold with dimensions (27.0 x 27.0 x 0.5 cm^3) (length x width x thickness) and pre-pressed (0.49 MPa, 10 min) in a laboratory environment maintained at 25 °C and 55% relative humidity (RH). Thermal consolidation was performed using a hydraulic hot press (185 °C, 20 MPa, and 18 min). The fabricated particleboards were cooled and conditioned at ambient conditions for one week before testing, as shown in Fig. 2. All composites were manufactured as single-layer particleboards. For each adhesive formulation, five replicate particleboards were fabricated and evaluated to ensure the reliability and reproducibility of the results according to JIS A-5908 (2015), ASTM D1037 (1999), and EN 319 (1993)/EN 310 standards (1993). The masses of air, *Rh.* spp. particles, adhesive mixtures, and distilled water were measured using Eq. 1,

$$M_{air} = \rho V$$
$$M_{Rh.\ spp.} = W_{Rh.\ spp.}\% \times M_{air} \times (1 + MC\%_{Rh.\ spp.})$$
$$M_{DSF-SPC-SPI} = W_{DSF-SPC-SPI}\% \times M_{air} \times (1 + MC\%_{DSF-SPC-SPI})$$
$$M_W = W_W\% \times M_{air} - [(M_{Rh.\ spp.} \times MC\%_{Rh.\ spp.}) + (M_{DSF-SPC-SPI} \times MC\%_{DSF-SPC-SPI})] \quad (1)$$

where M_{air}, ρ, and V denote air mass (g), composite density (g/cm^3), and volume (cm^3). $M_{Rh.\ spp.}$, $W_{Rh.\ spp.}\%$, and $MC\%_{Rh.\ spp.}$ represent the mass (g), weight fraction (dimensionless), and moisture content (%) of *Rh.* spp. particles. $M_{DSF-SPC-SPI}$, $W_{DSF-SPC-SPI}\%$, and $MC\%_{DSF-SPC-SPI}$ denote the corresponding properties of the adhesive mixtures. M_W and $W_W\%$ indicate the mass (g) and weight fraction (dimensionless) of distilled water.



Fig. 2. Manufactured composite particleboards

The prepared composite particleboards were sectioned into labeled test specimens and are presented in Fig. 3.

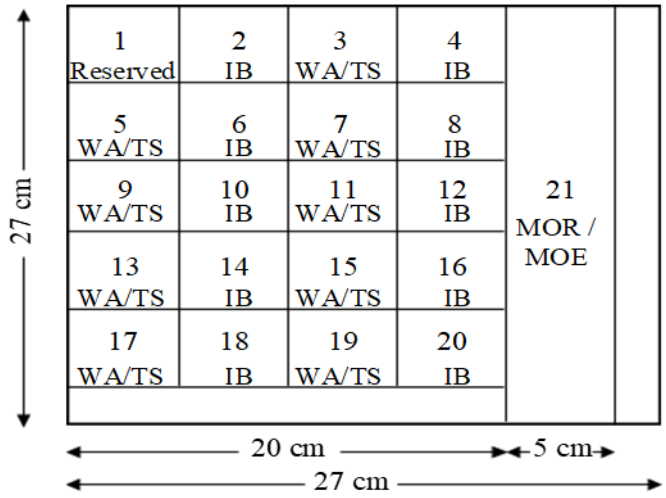


Fig. 3. Schematic representation of specimen preparation; test specimens were collected from multiple locations across each particleboard to account for composite heterogeneity.

Specimen 1 was set aside for other tests, while specimens 2, 4, 6, 8, 10, 12, 14, 16, 18, and 20 were used for internal bonding strength (IBS) testing. Specimens 3, 5, 7, 9, 11, 13, 15, 17, and 19 were designated for water absorption (WA) and thickness swelling (TS) measurements. Specimen 21 was used to evaluate flexural properties (MOR-modulus of rupture; MOE-modulus of elasticity). All measured parameters are presented as mean ± standard deviation (SD), as indicated in the figures and tables. In addition, statistical analyses were conducted to evaluate differences between the unmodified and modified adhesive variants.

Fourier Transform Infrared (FTIR) Spectrometry Analysis

The FTIR spectra were collected on an IRPrestige-21 spectrophotometer (Shimadzu, Japan) in diffuse reflectance mode. Prior to analysis, the cured adhesive and composite samples were oven-dried, finely ground, and sieved to obtain a homogeneous powder. Approximately 1 mg of sample was thoroughly mixed with KBr (100 mg) and pressed into disc pellets (thickness: 0.5 mm, diameter: 12.71 mm) at 32 MPa for 3 min, as shown in Fig. 4. Spectra were recorded over the range of 4000 to 400 cm^{-1} at a resolution of 4 cm^{-1} with 32 scans.

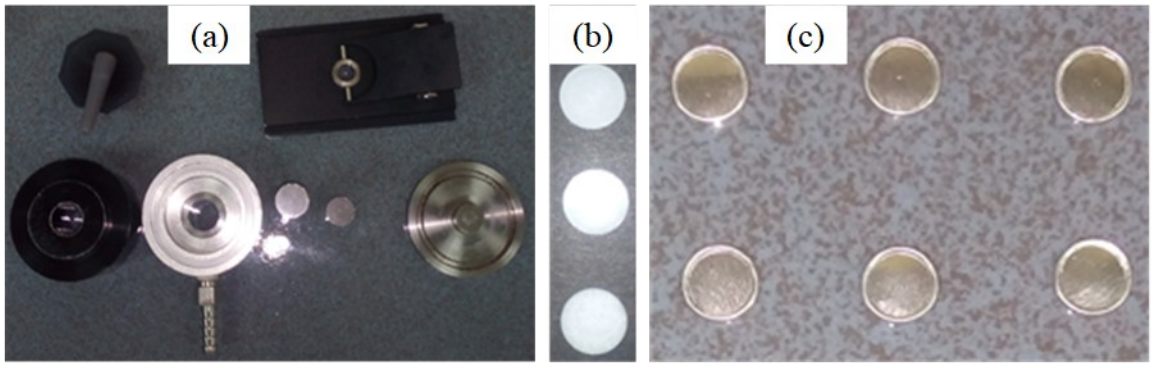


Fig. 4. FTIR spectroscopy: (a) Metal moulds used for making the pellets, (b) Sample pellets, and (c) Disc pellets of crimped samples

Thermal Properties

Thermogravimetric (TG) and derivative thermogravimetric (DTG) analyses were performed on an STA 6000 (Perkin-Elmer, USA) under a nitrogen atmosphere. An empty aluminum pan served as the reference. A 5 mg ground sample was sealed in an aluminum pan. The sample was heated from 30 to 900 °C at 10 °C/min (20 mL/min N_2) with a 5 min hold at 900 °C. Mass loss was recorded as a function of temperature, and the peak temperature in the DTG curve was used as an indicator of thermal stability.

Field Emission Scanning Electron Microscopy (FESEM) and Energy Dispersive X-ray (EDX) Analysis

The morphology of the composites was examined using an FESEM (FEI Quanta FEG-650, Netherlands). Sample cross-sections (0.5 x 0.5 x 0.5 cm^3) were oven-cured at 120 °C, mounted on metal straps, and sputter-coated with approximately 0.5 µm of gold (~60%) for 30 s at 45 mA (Polaron SC515, UK). Micrographs were acquired at 5 to 20 kV, with a 30° tilt and 500x magnification. Chemical compositions were determined and compared with water and other commercial tissue substitute biomaterials using the EDX system integrated with the FESEM.

Density

Specimens (5.0 x 5.0 x 0.5 cm^3) were prepared and labeled accordingly, and ρ with its associated uncertainties was calculated using Eq. 2,

$$\rho\ (gcm^{-3}) = \frac{m\ (g)}{l \times w \times h\ (cm^3)}$$

$$d\rho\ (gcm^{-3}) = (\frac{dm}{m} + \frac{dl}{l} + \frac{dw}{w} + \frac{dh}{h})\rho \quad (2)$$

where m, l, w, and h denote the respective mass (g), length (cm), width (cm), and thickness (cm), while dm, dl, dw, and dh represent the respective uncertainties.

Moisture Content (MC)

Each sample was weighed in a petri dish, oven-dried at 105 °C for 24 h, then cooled in a desiccator for 10 min. The final weight was recorded, and MC (%) was evaluated using Eq. 3:

$$MC = \frac{W_{(petri+sample)before\ oven-dry} - W_{(petri+sample)after\ oven-dry}}{W_{(petri+sample)before\ oven-dry} - W_{petri\ dish}} \times 100\% \quad (3)$$

Solid Content (SC)

Approximately 3 g of each sample was placed in an aluminum pan and oven-dried at 103 ± 2 °C for 24 h. The weight was recorded, and the average SC (%) was calculated using Eq. 4:

$$SC = \frac{W_{(pan+sample)after\ oven-dried} - W_{aluminum\ pan}}{W_{(pan+sample)before\ oven-dried} - W_{aluminum\ pan}} \times 100\% \quad (4)$$

Internal Bonding Strength (IBS)

Specimens (5.0 x 5.0 x 0.5 cm^3) were prepared as shown in Figs. 3 and 5.

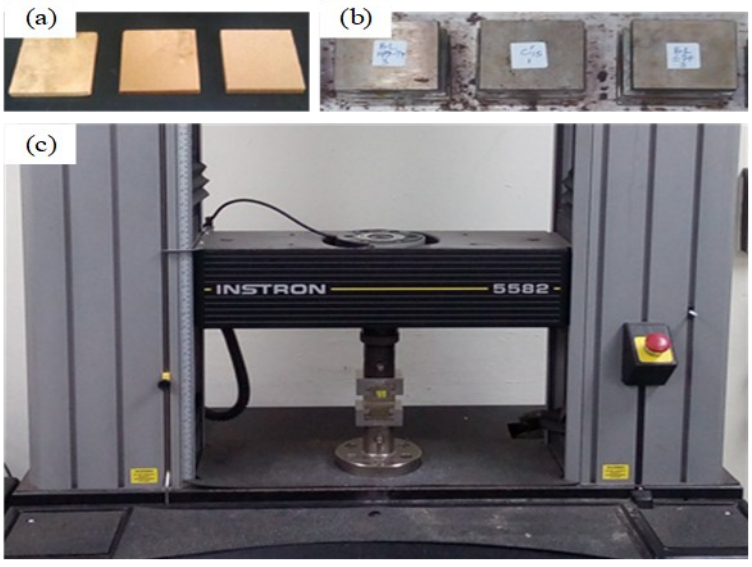


Fig. 5. Sample setup for IBS testing and specimen configuration: (a) Composite particleboard test samples, (b) IBS mould blocks, and (c) UTM-5582 with integrated test samples

The IBS was measured using an INSTRON universal testing machine (UTM-5582, USA) at a crosshead speed of 2 mm/min. Samples were bonded between preheated metal blocks (150 ℃) with adhesive applied evenly to both surfaces and then conditioned at room temperature for 24 h. The bonded samples were mounted in tensile fixtures, and load was applied perpendicular to the particleboard surface until failure. The maximum load at fracture was recorded, and IBS was assessed using Eq. 5,

$$IBS = \frac{F_{max}}{2wl} \quad (5)$$

where l is the span (cm) between two supporting points, and w is the width (cm) of the testing sample.

Flexural Properties (MOR and MOE)

For the bending test, specimens measuring 27 x 5 x 0.5 cm^3 were prepared as shown in Figs. 3. and 6. The 3-point bending test was conducted with a span-to-depth ratio of 52:1 and a crosshead speed of 10 mm/min. The support span was set to 15 cm, and the load was applied centrally until failure. The collected load-deflection data were used to calculate MOR and MOE (Eqs. 6 and 7),

$$MOR = \frac{3F_{max}l}{2wh^2} \quad (6)$$

$$MOE = \frac{F_{max}l^3}{4wh^3 s_d t} \quad (7)$$

where F_{max}, l, h, t, and s_d represent breaking force (N), support point spacing (cm), thickness (cm), time (s), and downward displacement speed (cm/s). The mechanical parameters were then assessed through various tests. The IBS and MOR were evaluated according to JIS A-5908 (2015) Types 8, 13, and 18, EN 319 (1993), and EN 310 (1993), while the MOE was determined in accordance with ASTM D1037 (1999) M-2 and EN 310 (1993).



Fig. 6. Sample orientation for MOR and MOE testing

Water Absorption and Thickness Swelling Tests

Rectangular specimens (5.0 x 5.0 x 0.5 cm^3), as shown in Fig. 3, were prepared and oven-dried at 105 °C for 24 h. The initial weight (W_0) and thickness (h_0) were measured with an accuracy of 1 x 10^{-3} g and 1 x 10^{-2} mm, respectively. The specimens were then immersed horizontally in distilled water at 23 ± 2 °C for 24 h. After immersion, the weight gain (W_{24}) and thickness (h_{24}) were immediately measured. Water absorption (WA_{24}) and thickness swelling (TS_{24}) were calculated as percentage changes using Eqs. 7 and 8:

$$WA_{24} = \frac{W_{24} - W_0}{W_0} \times 100\% \quad (7)$$

$$TS_{24} = \frac{h_{24} - h_0}{h_0} \times 100\% \quad (8)$$

RESULTS AND DISCUSSION

FTIR Analysis

The FTIR spectra of DSF-SPC-SPI/*Rh.* spp. and NaOH/IA-PAE-modified composites exhibited consistent chemical transformations that were indicative of cross-linking and interfacial enhancement.

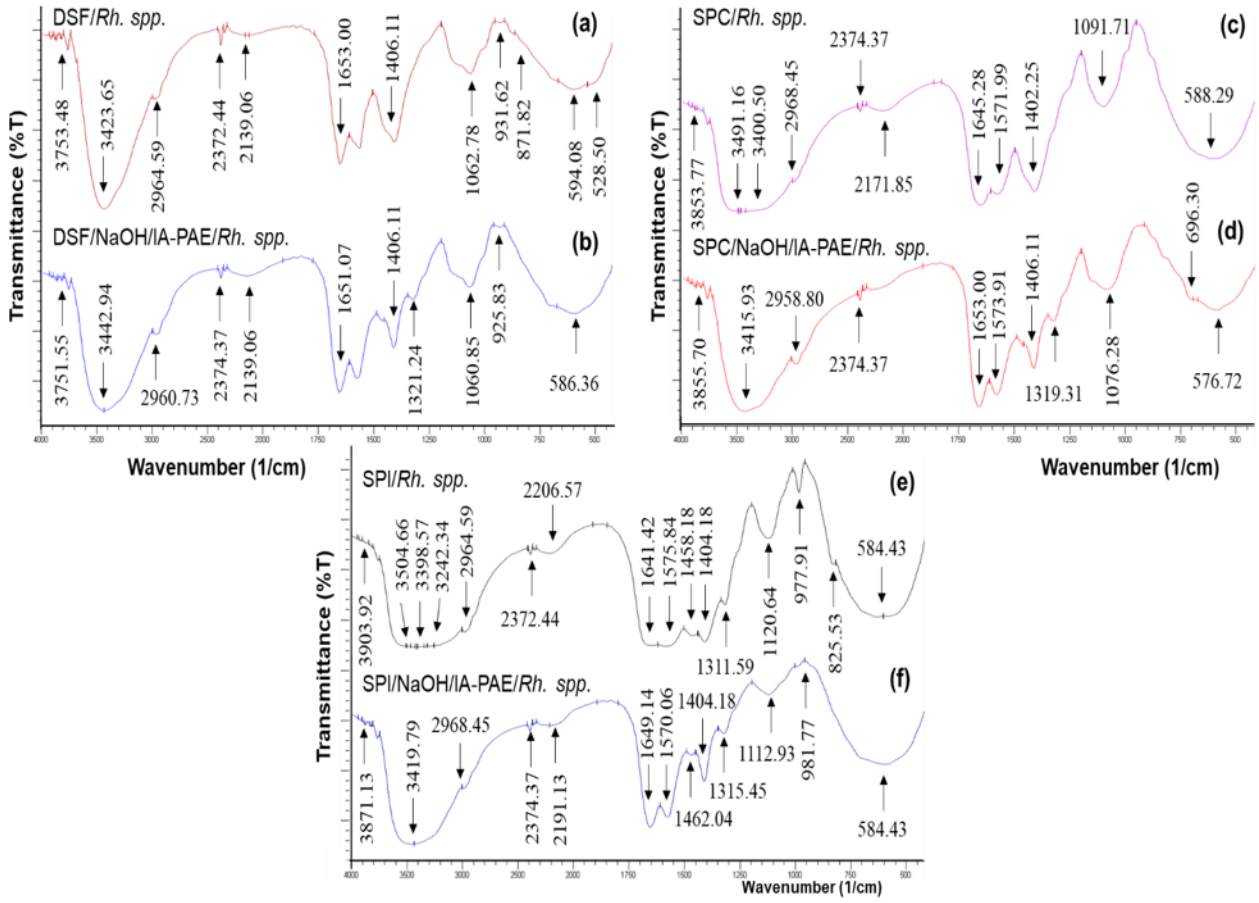


Fig. 7. FTIR spectra of composite adhesives, revealing the functional groups and structural changes after alkaline treatment and cross-linking: (a) DSF/*Rh* spp., (b) DSF/NaOH/IA-PAE/*Rh.* spp., (c) SPC/*Rh.* spp., (d) SPC/NaOH/IA-PAE/*Rh.* spp., (d) SPI/*Rh.* spp., and (e) SPI/NaOH/IA-PAE/*Rh.* spp.

Unmodified adhesive variants as shown in Figs. 7a, 7c, and 7e displayed broad O–H/N–H stretching (3240 to 3500 cm^{-1}), amide I (1641 to 1653 cm^{-1}), amide II (1562 to 1572 cm^{-1}), and C–O bands (1062 to 1091 cm^{-1}), indicating strong hydrogen bonding between DSF/SPC/SPI and lignocellulosic components, consistent with typical protein-fiber interactions (Chen *et al.* 2013; Anil and Trina 2019). After NaOH/IA-PAE treatment, notable spectral changes occurred and are presented in Figs. 7b, 7d, and 7f. The O–H/N–H band (3416 to 3443 cm^{-1}) generally decreased, suggesting hydroxyl consumption and stronger intermolecular interactions. Amide I band shifted to higher wavenumbers (1649 to 1653 cm^{-1}) with increased intensity, while amide II bands (1570 to 1575 cm^{-1}) became more prominent, confirming protein structural changes and covalent cross-linking with IA-PAE (Samson *et al.* 2020). Increased C–N and bands in the 1319 to 1462 cm^{-1} region support the formation of new ester and ether linkages (Chen *et al.* 2025). The presence of ester groups could facilitate adhesion in bonding wood-based composites (Karliati *et al*. 2024). Carbohydrate peaks shifted from 1060 cm^{-1} to 1091 cm^{-1}, indicating NaOH-induced disruption of the lignocellulosic structure and improved access for cross-linking. The reduction in C–H stretching (2965 cm^{-1}) and lower C–O/C–O–C band intensity (1120 cm^{-1}) suggests restricted chain mobility and hydroxyl participation in bonding.

Thermal Analysis

Figure 8a shows the multi-stage degradation of TG analysis, with clear improvement after NaOH/IA-PAE modification. Initial weight loss below 100 °C (1 to 2%) resulted from moisture evaporation; the smaller loss in NaOH/IA-PAE-modified composites indicates reduced hygroscopicity due to effective cross-linking (Zou *et al.* 2024). In the 100 to 250 °C range, modified samples retained more mass (92 to 93%), reflecting restricted chain mobility and strengthened intermolecular interactions (Xu *et al.* 2024; Zou *et al.* 2024). During the main degradation stage (250 to 350 °C), which involves cellulose depolymerization and soy protein backbone cleavage, DSF-SPC-SPI/*Rh.* spp. composites demonstrate slightly higher weight retention (74 to 76% at 294 °C), whereas DSF-SPC-SPI/NaOH/IA-PAE/*Rh.* spp. composites display broader mass-loss curves, indicating a more uniform network that allows gradual energy release.

At higher temperatures (400 to 800 °C), treated composites consistently retained more residue (DSF/NaOH/IA-PAE: 33.2% at 550 °C; 26.1% at 722 °C; SPC/NaOH/IA-PAE: 31.1%), confirming improved carbon retention and reduced volatilization (Xu *et al.* 2024). Final char yields at 898 °C (DSF/NaOH/IA-PAE: 17.6%, SPC/NaOH/IA-PAE: 15.1%, SPI/NaOH/IA-PAE: 12.8%) further indicate enhanced structural compactness and thermal stability. The DTG results showed faster moisture release (30 to 70 °C) but lower degradation rates at 70 to 150 °C, indicating better intermediate stability, as depicted in Fig. 8b. In the 200 to 400 °C range, sharper peaks at slightly lower temperatures (−3.03% min^{-1}) suggested controlled, synchronized breakdown of cross-linked networks. At 700 to 900 °C, smoother degradation confirmed stabilized char formation, showing that modification redefined degradation pathways while enhancing thermal resilience.

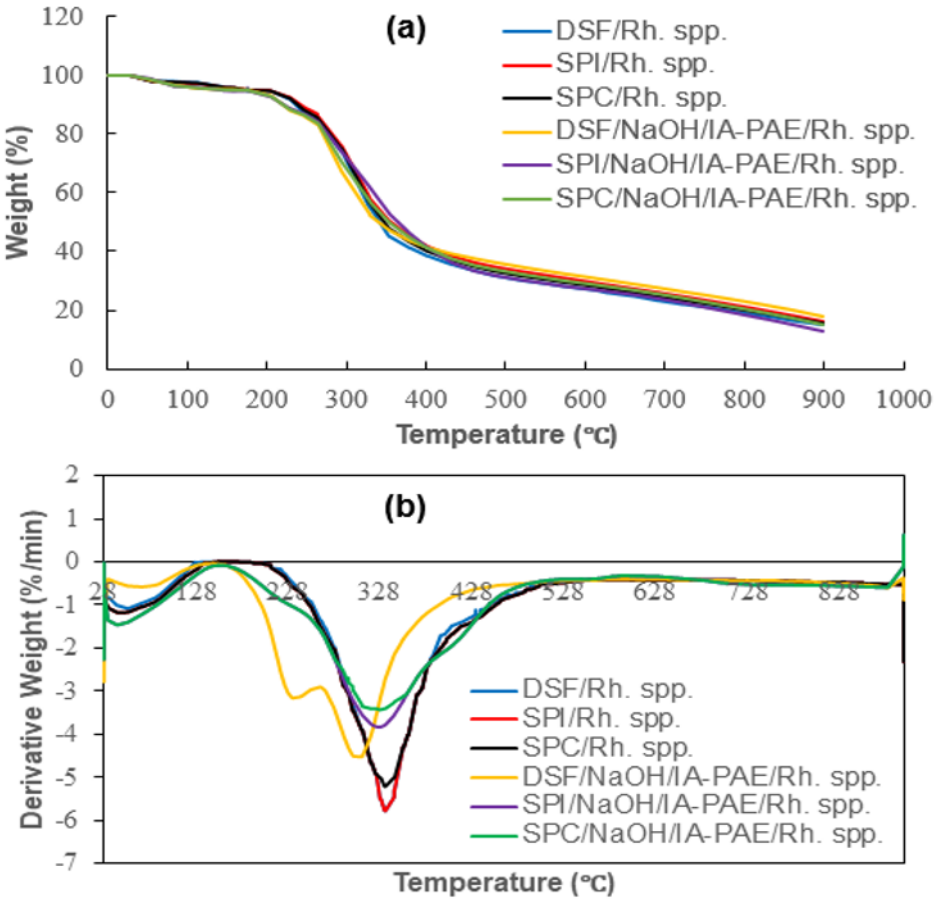


Fig. 8. (a) TG and (b) DTG profiles of soy protein particleboards; The plots compare unmodified (DSF, SPI, SPC) and NaOH/IA-PAE cross-linked composites, highlighting multi-stage thermal degradation

FESEM and EDX Analysis

Figure 9 illustrates improvements in microstructure and interfacial bonding across the adhesive composites. The DSF/*Rh.* spp.-bonded composite showed a heterogeneous, porous structure with uneven adhesive spread, noticeable voids, and noticeable particle pull-out, suggesting poor wetting and weak adhesion.

These findings are presented in Fig. 9a. SPC/*Rh.* spp. revealed slight improvement but remained porous, with visible gaps at the interface and predominant debonding failure, as shown in Fig. 9b. In contrast, SPI/*Rh.* spp. formed a more uniform matrix that effectively coated and connected particles, reducing voids and improving stress transfer, as evidenced by partial cohesive failure in Fig. 9c. Notable densification was observed after NaOH treatment, and IA-PAE crosslinking is presented in Fig. 9d, 9e and 9f. These modified adhesive variants had denser, more uniform structures with better binder continuity, reduced porosity, and fewer microcracks. Enhanced interfacial adhesion is reflected in smoother transitions and less debonding in wood composites (Xian-Qing *et al.* 2020). Smoother adhesive films often lead to greater adhesive-wood surface interaction by improving molecular interactions between the adhesive and *Rh.* spp. wood (Wibowo and Park 2021). Among all composite samples, SPI/NaOH/IA-PAE/*Rh.* spp. demonstrated the most integrated structure, featuring a dense interpenetrating network and ductile fracture characteristics (Samson *et al.* 2020; Tayo *et al.* 2025).

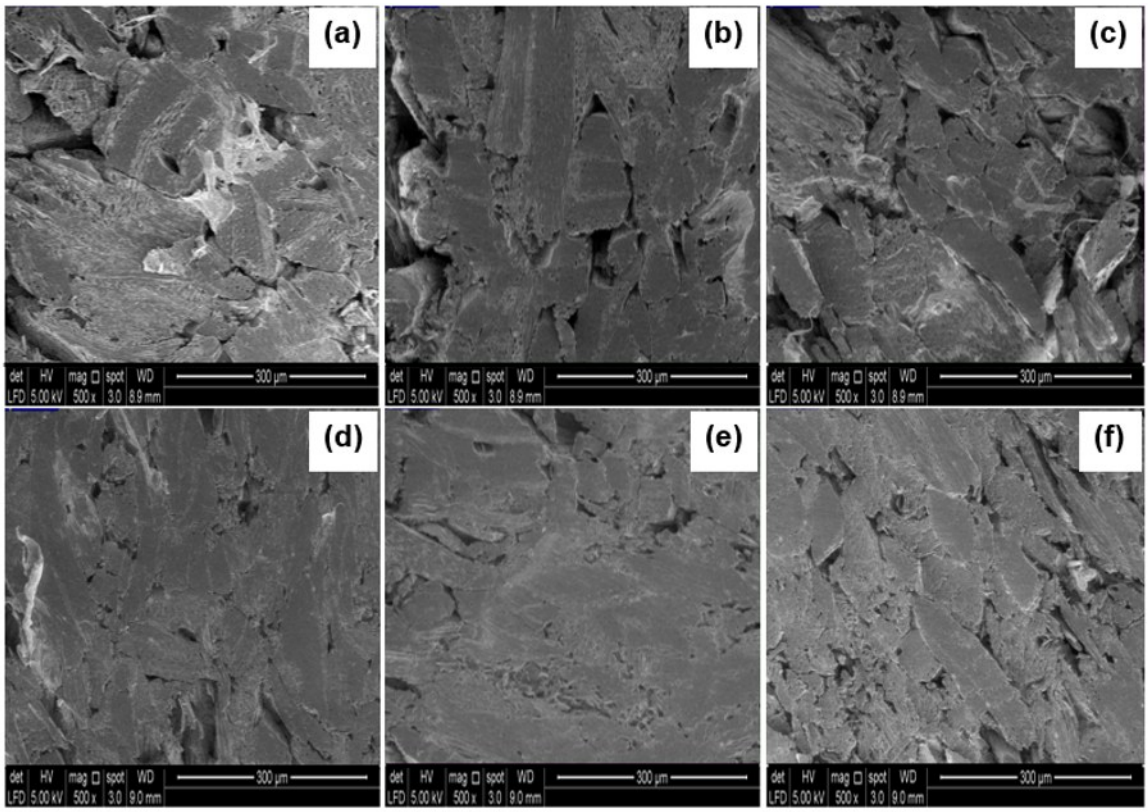


Fig. 9. FESEM micrographs of soy protein-bonded composite particleboards: (a) DSF/*Rh.* spp., (b) SPC/*Rh.* spp., (c) SPI/*Rh.* spp., (d) DSF/NaOH/IA-PAE/*Rh.* spp., (e) SPC/NaOH/IA-PAE/*Rh.* spp., and (f) SPI/NaOH/IA-PAE/*Rh.* spp.

The EDX spectra of the particleboards confirm a well-integrated organic-inorganic composite structure, as shown in Fig. 10. Table 1 summarizes the chemical composition of the composite particleboards and compares it with water, Perspex, and paraffin wax. Dominant carbon (C) and oxygen (O) peaks reflect the lignocellulosic framework and protein-based adhesive, indicating abundant functional groups for hydrogen bonding and cohesion within the network. Sodium (Na) peaks confirm NaOH treatment, suggesting improved protein unfolding and fiber surface activation. Pronounced calcium (Ca) and potassium (K) signals originated from natural biomass minerals and contributed to dimensional stability and ionic interactions within the matrix. Minor phosphorus (P) and sulfur (S) peaks confirm the presence of soy protein and the participation of amino acid residues in cross-linking.

The detection of chlorine (Cl) supports the successful integration of IA-PAE cross-linkers, indicating effective curing and network formation. Trace elements (Mg, Fe, Mn, and Zn) were present at low levels and were attributed to natural impurities.

The elemental composition of composite particleboards with 20 to 30 wt% IA-PAE indicated a synergistic bonding network that enhanced structural integrity and radiation-related performance, consistent with water and other commercial tissue substitute biomaterials (Watanabe and Constantinou 2006; Abuarra *et al.* 2014; Samson *et al.* 2020; Tayo *et al.* 2025).

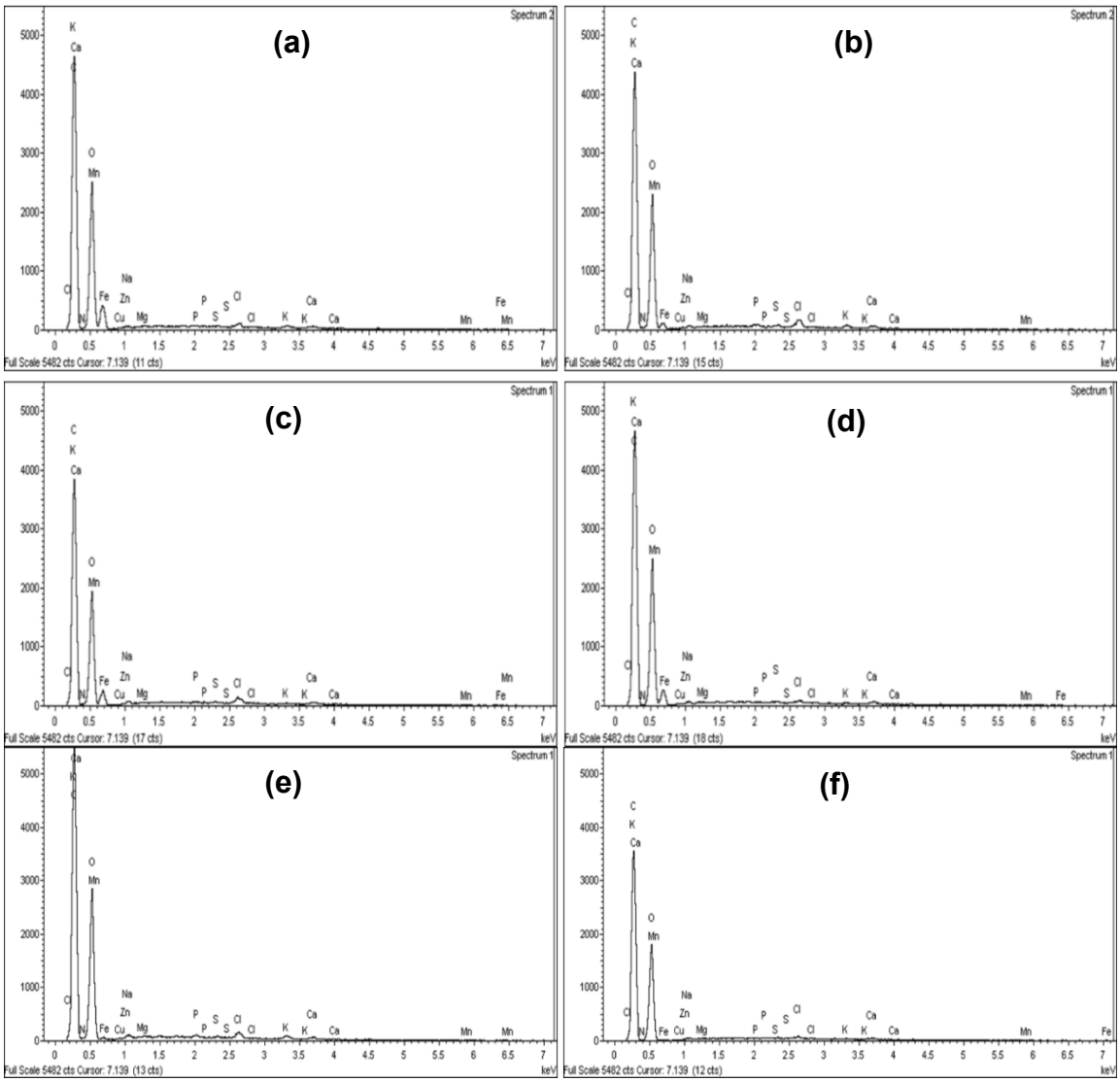


Fig. 10. EDX spectra of particleboards confirming the formation of a chemically integrated organic-inorganic composite network. (a) DSF/*Rh.* spp., (b) SPC/*Rh.* spp., (c) SPI/*Rh.* spp., (d) DSF/NaOH/IA-PAE/*Rh.* spp., (e) SPC/NaOH/IA-PAE/*Rh.* spp., and (f) SPI/NaOH/IA-PAE/*Rh.* spp.

Table 1. Comparison of Elemental Atomic Compositions

Composite	Weight Fraction of Element (%)												
	H	C	O	Na	Ca	K	P	S	Cl	Mg	Fe	Mn	Zn
DSF_0	-	52.99	45.82	0.18	0.13	0.20	0.10	0.08	0.27	0.05	-	0.10	-
SPC_0	-	53.45	45.26	0.17	0.20	0.23	0.11	0.10	0.48	-	-	-	-
SPI_0	-	53.39	45.96	0.18	0.12	0.10	0.08	0.03	0.09	0.04	-	-	-
DSF_{10}	-	53.06	46.38	0.19	0.16	0.03	-	0.03	0.05	-	0.05	-	0.05
SPC_{10}	-	53.75	45.49	0.14	0.21	0.08	-	0.04	0.11	0.05	0.10	0.03	-
SPI_{10}	-	53.28	46.05	0.13	0.10	0.15	-	0.03	0.13	0.04	0.05	-	0.04
DSF_{20}	-	53.73	45.02	0.19	0.14	0.18	0.12	0.05	0.32	0.04	0.07	0.05	0.09
SPC_{20}	-	54.05	45.22	0.10	0.10	0.07	0.05	0.04	0.18	0.05	0.05	0.04	0.05
SPI_{20}	-	54.23	44.58	0.30	0.18	0.05	0.04	0.05	0.32	0.03	0.07	0.06	0.09
DSF_{30}	-	53.80	45.47	0.14	0.18	0.08	0.04	0.06	0.14	0.02	0.04	-	0.03
SPC_{30}		53.71	45.50	0.19	0.13	0.06	0.03	0.05	0.15	0.02	0.06	0.10	-
SPI_{30}	-	53.98	43.91	0.12	0.11	0.11	0.09	0.07	0.11	0.04	1.25	0.17	0.04
Perspex[a]	8.05	59.98	31.97	-	-	-	-	-	-	-	-	-	-
Water[a]	11.11	-	88.89	-	-	-	-	-	-	-	-	-	-
Paraffin wax[b]	15.00	85.00	-	-	-	-	-	-	-	-	-	-	-
Polystyrene[c]	7.74	92.26	-	-	-	-	-	-	-	-	-	-	-

Note: DSF_0: DSF/*Rh.* spp. (unmodified DSF), SPC_0: SPC/*Rh.* spp. (unmodified SPC), SPI_0: SPI/*Rh.* spp. (unmodified SPI), DSF_{10}, DSF_{20}, DSF_{30}: DSF/NaOH/IA-PAE/*Rh.* spp., SPC_{10}, SPC_{20}, SPC_{30}: SPC/NaOH/IA-PAE/*Rh.* spp., SPI_{10}, SPI_{20}, SPI_{30}: SPI/NaOH/IA-PAE/*Rh.* spp. represents 0, 10, 20, and 30 wt% IA-PAE; [a] Watanabe and Constantinou (2006), [b] Abuarra *et al.* (2014), [c] Schoenfeld *et al.* (2015)

Physical Measurements

Physical properties are summarized in Figs. 11a, 11b, and 11c, highlighting the influence of NaOH/IA-PAE crosslinking on composite particleboard performance. The average densities of the developed *Rh.* spp. composite particleboards ranged from 0.94 ± 0.11 to 1.04 ± 0.20 g/cm^3, closely matching water density (1.0 g/cm^3), indicating compact structures with minimal voids in Fig. 11a. The unmodified adhesive variants showed slight variability, with SPC-based composites exhibiting the lowest density (0.94 ± 0.11 g/cm^3) and DSF-based particleboards the highest (1.04 ± 0.20 g/cm^3). Incorporation of NaOH/IA-PAE improved density uniformity (0.96 ± 0.10 to 1.03 ± 0.10 g/cm^3), suggesting enhanced particle packing and interfacial bonding without excessive densification, comparable to commercial tissue biomaterials (Samson *et al.* 2020).

Figure 11b depicts the moisture content range (6.51 ± 0.19 to 8.06 ± 0.50 %), which complied with JIS A-5908 (2015) requirements (5 to 13%) and aligned with reported values for bio-based particleboards (Karliati *et al.* 2024). The unmodified adhesive variants exhibited moisture contents (7.81 ± 0.43 to 8.06 ± 0.50 %), whereas cross-linked samples revealed a gradual reduction, particularly at higher IA-PAE concentrations. The lowest value (6.51 ± 0.19%) was observed for SPI/NaOH/IA-PAE (20%), which can be attributed to reduced accessibility of hydrophilic groups and improved network formation (Samson *et al.* 2023).

Solid content increased markedly from 30.70 ± 1.45 to 33.09 ± 0.91% in untreated composites to 33.11 ± 1.01 to 37.73 ± 0.40 % after crosslinking in Fig. 11c, indicating enhanced adhesive concentration that supports interfacial bonding and composite development. The highest value was achieved by SPI/NaOH/IA-PAE (20%), reflecting

efficient crosslinking and improved retention of solid constituents. This suggests that the crosslinking system promotes better polymer integration and reduces material loss during processing. Higher solid content is generally associated with improved mechanical integrity and durability, aligning these composites with the performance expectations of commercial bio-based particleboards (Samson *et al.* 2023; Karliati *et al.* 2024).

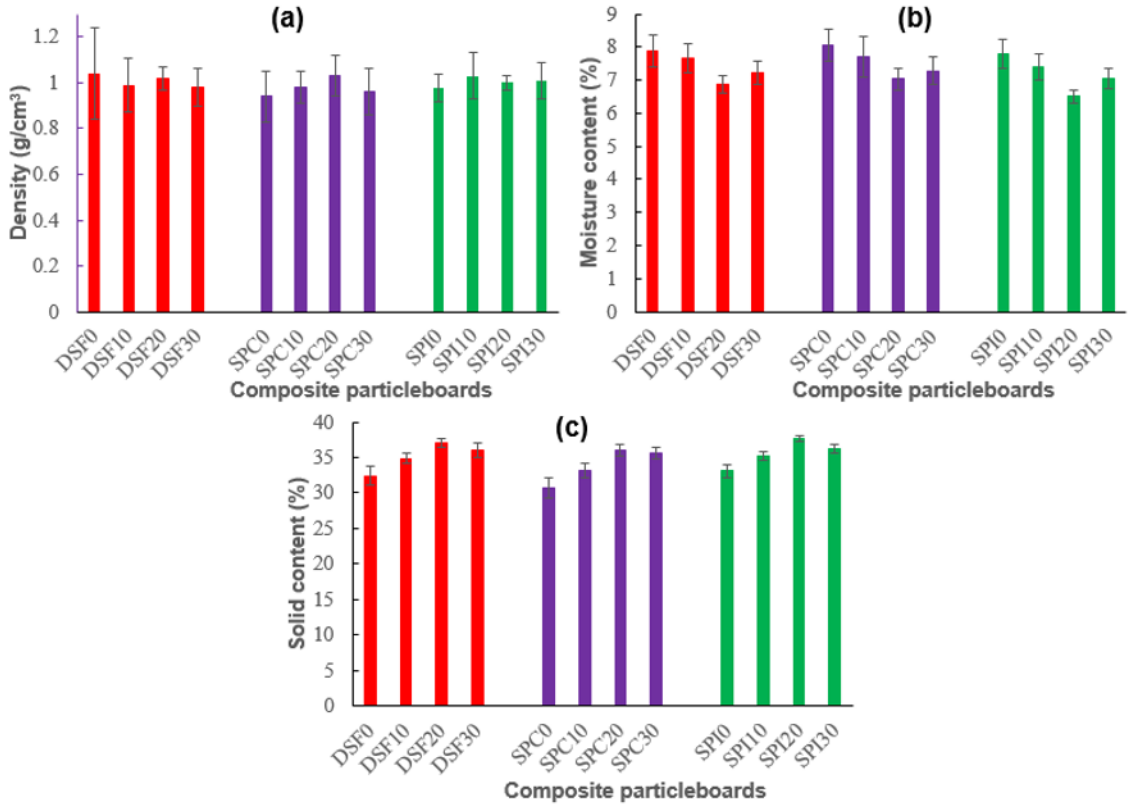


Fig. 11. Physical parameters of composite particleboards: (a) Density, (b) Moisture content, and (c) Solid content

Mechanical Properties

NaOH/IA-PAE crosslinking substantially enhanced mechanical performance, as shown in Fig. 12a, 12b, and 12c. The IBS ranged from 0.41 ± 0.08 to 0.73 ± 0.01 MPa, with all composites exceeding the JIS A-5908 (2015) minimum requirements for Type 8 (0.15 MPa), Type 13 (0.20 MPa), and Type 18 (0.30 MPa), as well as the EN 319 (1993) requirement for Type P2 (0.35 MPa) particleboards (Fig. 12a). Unmodified adhesive variants exhibited moderate IBS (0.41 ± 0.08 to 0.49 ± 0.07 MPa), whereas cross-linked composites showed substantial improvement, reaching a maximum of 0.73 ± 0.01 MPa for SPI/NaOH/IA-PAE/*Rh.* spp. with 20% IA-PAE. This enhancement is attributed to the formation of a dense three-dimensional network that strengthens interfacial adhesion and cohesive integrity, consistent with recent reports on cross-linked bio-based adhesive variants (Karliati *et al.* 2024). FTIR results further indicated the formation of additional interactions among DSF/SPC/SPI, IA-PAE, and *Rh.* spp. constituents, which enhanced matrix-filler interfacial bonding. The improved interfacial adhesion facilitated more efficient stress transfer and reduced interfacial debonding, thereby contributing to the observed mechanical performance enhancement.

Similarly, MOR increased from 10.15 ± 1.18 to 10.91 ± 1.01 MPa (unmodified adhesive variants) to 17.80 ± 1.07 to 19.21 ± 0.50 MPa at 20% IA-PAE in Fig. 12b, satisfying the performance range for higher-grade composites (JIS A-5908: Type 18, EN 310: Type P2). Likewise, the MOE improved from 3.91 ± 1.01 to 4.89 ± 0.64 GPa to a maximum of 7.70 ± 0.33 GPa, as shown in Fig. 12c, indicating increased stiffness and load-bearing capacity in agreement with ASTM D1037 (1999) and EN 310 (1993) standards. The figures indicate that these improvements were associated with better stress transfer efficiency and stronger matrix-filler interactions induced by crosslinking. However, at 30% IA-PAE, slight reductions in IBS, MOR, and MOE were observed, suggesting that excessive crosslinking may introduce brittleness or restrict effective stress distribution. The 20% IA-PAE provided the optimal balance of strength and stiffness, particularly in SPI-based composites. These results align with recent findings that intermediate cross-linker concentrations maximize mechanical performance in bio-based particleboards (Karliati *et al.* 2024; Xu *et al.* 2024; Zuber *et al.* 2025; Samson *et al.* 2025; Tayo *et al.* 2025; Baskaran *et al.* 2026; Marta *et al.* 2026; Younesi-Kordkheili and Pizzi 2026).

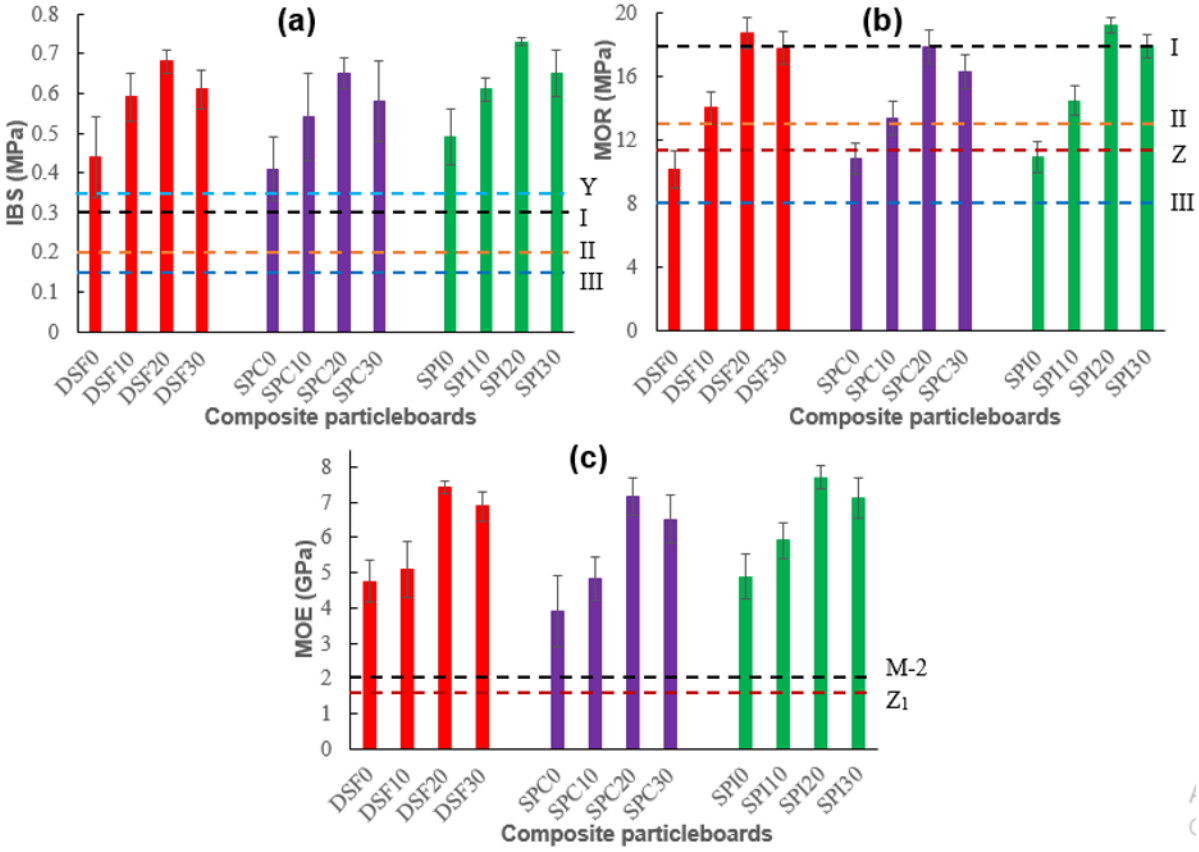


Fig. 12. Mechanical properties, showing compliance with reference standards and peak performance at 20% IA-PAE: (a) IBS, (b) MOR, and (c) MOE. I: Type 18, II: Type 13, and III: Type 8 (JIS A-5908 2015); M-2 (ASTM D1037 1999); Y: Type P2 (EN 319 1993); Z/Z_1: EN 310:1993

Determination of WA and TS

The unmodified adhesive variants exhibited high WA (32.41 ± 2.66 to 36.11 ± 3.03 %) and TS (25.38 ± 2.07 to 30.08 ± 4.01 %), as shown in Fig. 13, reflecting the hydrophilic nature of soy proteins and lignocellulosic particles. These values exceed the typical 12%

maximum allowable swelling limit associated with the JIS A-5908 (2015) and ASTM D1037 (1999) standards, indicating poor moisture resistance in unmodified adhesive variants (ASTM D1037 1999; JIS A 5908 2015). Incorporating NaOH/IA-PAE markedly reduced WA and TS. At 10% cross-linker loading of IA-PAE, WA was decreased to 27.23 ± 2.01 to 29.32 ± 1.78% and TS to 17.84 ± 2.63 to 21.30 ± 2.99%, demonstrating enhanced water resistance due to partial network formation. A more pronounced enhancement was observed at 20% IA-PAE, where WA further decreased to 20.09 ± 1.23 to 21.17 ± 1.21% and TS (10.07 ± 1.59 to 10.50 ± 2.32%), consistent with reference standards (ASTM D1037 1999; JIS A 5908 2015). This improvement is attributed to the formation of a dense cross-linked network that limits hydroxyl group accessibility and restricts water penetration. At 30% IA-PAE, slight increases in WA and TS were observed, suggesting that excessive crosslinking may induce structural rigidity and micro-void formation.

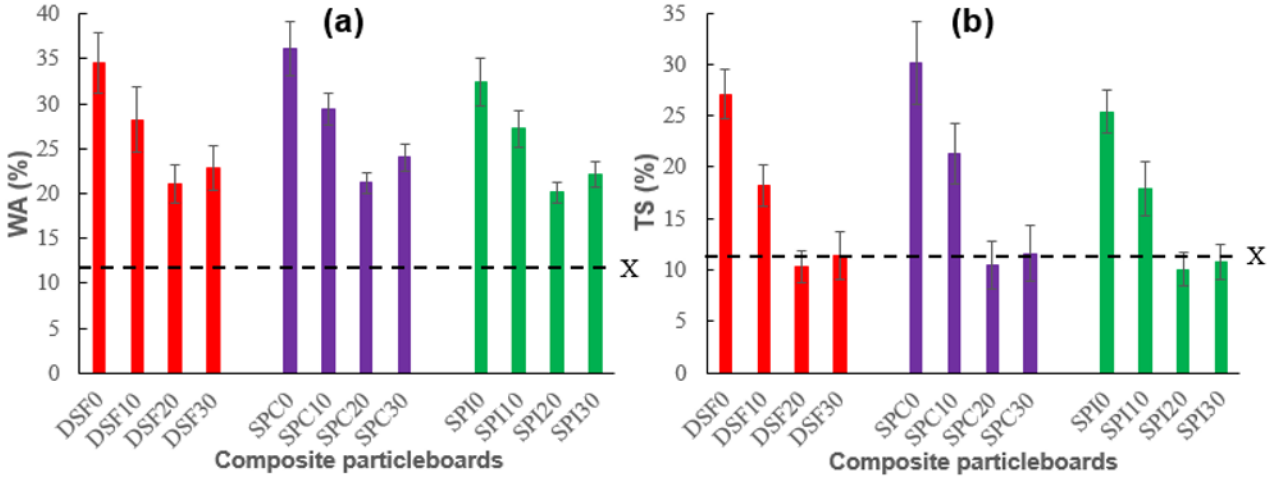


Fig. 13. Dimensional stability: (a) WA and (b) TS. X: JIS A-5908 limits

CONCLUSIONS

1. Sodium hydroxide/itaconic acid/poly(amidoamine epichlorohydrin) (NaOH/IA-PAE) crosslinking effectively enhanced the performance of defatted soy flour/soy protein concentrate/soy protein isolate (DSF/SPC/SPI)-bonded *Rhizophora* spp. wood composite particleboards, demonstrating that particleboard properties can serve as reliable indicators of adhesive bonding performance.
2. Structural analyses confirmed the formation of a dense, cross-linked network, with improved interfacial bonding and reduced hydroxyl accessibility. This led to increased thermal stability, as evidenced by higher residual mass and enhanced degradation behavior.
3. The composites exhibited densities comparable to water (1.0 g/cm^3) and to other commercial tissue substitute biomaterials, with moisture content within JIS A-5908 (2015) limits.
4. Mechanical properties exceeded standard requirements (EN 319 (1993)/EN 310 (1993); ASTM D1037 (1999); JIS A-5908 (2015)), with optimal performance at 20%

IA-PAE (IBS: 0.73 ± 0.01 MPa; MOR: 19.21 ± 0.50 MPa; MOE: 7.70 ± 0.33 GPa). Dimensional stability also improved substantially.

5. The 20% IA-PAE achieved the best balance of properties, highlighting its suitability for advanced bio-based applications and potential for tissue-equivalent materials in radiation-related contexts, which require further radiation attenuation and shielding studies.

ACKNOWLEDGMENTS

The authors would like to thank the scientific and technical support provided by the Wood Processing Laboratory, School of Industrial Technology, Universiti Sains Malaysia, Malaysia. This work was also funded by the Fundamental Research Grant Scheme (FRGS/1/2024/STG07/UKM/02/4) from the Ministry of Higher Education (MOHE), Malaysia.

AUTHOR'S CONTRIBUTION STATEMENT

D.O.S.: Conceptualization, Methodology, Software, Data curation, Validation, Writing-original draft preparation, Writing – Reviewing and Editing. S.H.Z.: Conceptualization, Data curation, Methodology, Visualization, Funding acquisition, Writing-original draft preparation, Writing – Reviewing and Editing. S.N.A.M.Z.: Conceptualization, Methodology, Validation, Writing – Reviewing and Editing. M.S.A.F.: Conceptualization, Methodology, Visualization, Writing – Reviewing and Editing. A.B.O.: Conceptualization, Methodology, Validation, Writing – Reviewing and Editing. M.Z.A.A.: Conceptualization, Methodology, Visualization, Writing – Reviewing and Editing. P.G.: Conceptualization, Methodology, Validation, Writing – Reviewing and Editing. S.B.L.: Conceptualization, Methodology, Visualization, Writing – Reviewing and Editing.

USE OF GENERATIVE AI

ChatGPT (GPT-5) was employed primarily for rephrasing sentences and elaboration to enhance clarity and readability, and for grammar checking to ensure linguistic accuracy in academic and professional writing.

REFERENCES CITED

Abuarra, A., Hashim, R., Bauk, S., Kandaiya, S., and Tousi, E. T. (2014). "Fabrication and characterization of gum Arabic bonded *Rhizophora spp*. particleboards," *Materials & Design* 60, 108-115. https://doi.org/10.1016/j.matdes.2014.03.032

Anil, N. N., and Trina, G. D. (2019). "Crosslinked thermoset resins and methods thereof," U. S. Patent No. 10,179,807.

Anugrah, M. A., Suryani, S., Ilyas, S., Mutmainna, I., Fahri, A. N., and Tahir, D. (2020). "Composite gelatin/*Rhizophora spp*. particleboards/PVA for soft tissue phantom

applications," *Radiat. Phys. Chem.* 173, article 108878. https://doi.org/10.1016/j.radphyschem.2020.108878

ASTM D1037-99 (1999). "Standard test methods for evaluating properties of wood-base fibre and particle panel materials," ASTM International, West Conshohocken, PA, USA.

Banjade, D. P., Shrestha, S. L., Shukri, A., Tajuddin, A. A., and Bhat, M. (2002). "A simplified approach for exit dose *in vivo* measurements in radiotherapy and its clinical application," *Australasian Physical and Engineering Sciences in Medicine* 25(3), 110-118. https://doi.org/10.1007/BF03178771

Baskara, U. R., Zakaria, S. N. A. M., Zuber, S. H., Hadi, M. F. R. A., Hashikin, N. A. A., and Fadzil, M. S. A. (2026). "Soy-lignin bonded *Rhizophora spp*. as a bio-based phantom: Impact of adhesives on attenuation," *BioResources* 21(2), 3394-3416. https://doi.org/10.15376/biores.21.2.3394-3416

Chen, H., Zhang, Y., Tan, Y., Shao, J., Li, X., Bai, M., Gong, S., Liu, T., and Li, J. (2025). "A xylem fiber cell walls-inspired high-performance and multifunctional soy protein isolate adhesive with a double cross-linked strengthening network," *Int. J. Adhes.* 138, article 103928. https://doi.org/10.1016/j.ijadhadh.2024.103928

Chen, X., Ru, Y., Chen, F., Wang, X., Zhao, X., and Ao, Q. (2013). "FTIR spectroscopic characterization of soy proteins obtained through AOT reverse micelles," *Food Hydrocolloid.* 31(2), 435-437. https://doi.org/10.1016/j.foodhyd.2012.11.017

Chien, K. B., and Shah, R. N. (2012). "Novel soy protein scaffolds for tissue regeneration: Material characterization and interaction with human mesenchymal stem cells," *Acta Biomaterialia* 8(2), 694-703. https://doi.org/10.1016/j.actbio.2011.09.036

EN 310 (1993). "Wood-based panels–determination of modulus of elasticity in bending and of bending strength," European Commission for Standardization, Brussels, Belgium.

EN 319 (1993). "Particleboards and fiberboards–determination of tensile strength perpendicular to the plane of the board," CEN-European Committee for Standardization, Brussels, Belgium.

Frihart, C. R., and Satori, H. (2013). "Soy flour dispersibility and performance as wood adhesive," *J. Adhes. Sci. Technol.* 27, 2043-2052. https://doi.org/10.1080/01694243.2012.696948

Gao, D., Fan, B., Zhang, B., Mi, Y., Zhang, Y., and Gao, Z. (2019). "Storage stability of polyamidoamine- epichlorohydrin resin and its effect on the properties of defatted soybean flour-based adhesives," *Int. J Adhes. Adhes.* 91, 92-101. https://doi.org/10.1016/j.ijadhadh.2019.03.006

Gui, C., Wang, G., Wu, D., Zhu, J., and Liu, X. (2013). "Synthesis of a bio-based polyamidoamine- epichlorohydrin resin and its application for soy-based adhesives," *Int. J. Adhes. Adhes.* 44, 237-242. https://doi.org/10.1016/j.ijadhadh.2013.03.011

Hamid, P. N. K. A., Yusof, M. F. M., Hashim, R., and Tajuddin, A. A. (2018). "Characterization and attenuation properties of corn starch-bonded *Rhizophora spp*. particleboards as water equivalent phantom material at 16.59-25.26 XRF photons and ^{99m}Tc gamma energies," *Int. J. Environ. Engr.* 9(3-4), 254-270. https://doi.org/10.1504/IJEE.2018.097519

Hemmilä, V., Adamopoulos, S., Karlsson, O., and Kumar, A. (2017). "Development of sustainable bio-adhesives for engineered wood panels – A review," *RSC Adv.* 7(61), 38604-38630. https://doi.org/10.1039/c7ra06598a

JIS A-5908 (2015). "Japanese industrial standard for particleboards, Standardization Promotion Department," Japanese Standards Association, Tokyo, Japan.

Karliati, T., Lubis, M. A. R., Dungani, R., Maulani, R. R., Hadiyane, A., Rumidatul, A., Antov, P., Savov, V., and Lee, S. H. (2024). "Performance of particleboard made of agroforestry residues bonded with thermosetting adhesive derived from waste styrofoam," *Polymers (Basel)* 16(4), article 543. https://doi.org/10.3390/polym16040543

Marta, H., Indrianti, N., Aziza, A. J. N., Sholichah, E., Budiati, T., Sarifudin, A., Cahyana, Y., Sukri, N., and Pangawikan, A. D. (2026). "Enhancing corn starch-poly(vinyl alcohol) and glycerol composite films with citric acid cross-linking mechanism: A green approach to high-performance packaging materials," *J. Renew. Mater.* 14(1), 1-21. https://doi.org/10.32604/jrm.2025.02025-0145

Ng, P. K., Sivasothi, N., and Morgany, T. (1999). "Guide to the mangroves of Singapore I: The ecosystem and plant diversity," *Singapore Science Centre* 1999, 150-151.

Rowell, R. M., Pettersen, R., and Tshabalala, M. A. (2013). "Cell wall chemistry," in: *Handbook of Wood Chemistry and Wood Composites*, R. M. Rowell (ed.), CRC Press, Boca Raton, FL, USA, pp. 64-65.

Samson, D. O., Mat Jafri, M. Z., Hashim, R., Sulaiman, O., Aziz, M. Z. A., Yusof, M. F. M., and Shukri, A. (2020). "*Rhizophora spp*. particleboards incorporating defatted soy flour bonded with NaOH/IA- PAE: Towards a water equivalent phantom material," *Radiat. Phys. Chem.* 176, article 109057. https://doi.org/10.1016/j.radphyschem.202.109057

Samson, D. O., Shukri, A., Hashikin, N. A. A., Zuber, S. H., Addo Buba, A. D., Aziz, M. Z. A., Hashim, R., Yusof, M. F. M., Gemanam, S. J., and Samson, P. A. (2023). "Performance of natural product-based materials as adhesives in the fabrication of mangrove wood composites," *Heliyon* 9(1), article e13032. https://doi.org/10.1016/j.heliyon.2023.e13032

Samson, D. O., Zuber, S. H., Shukri, A., Aziz, M. Z. A., Biodun, A. D., Fadzil, M. S. A., Yahya, N. A., and Buba, A. D. A. (2025). "New alternative equivalent phantom materials developed for radiotherapy applications," *J. Phys.- IOP Conf. Series* 2944, article 012012. https://doi.org/10.1088/1742-6596/2944/1/012012

Schoenfeld, A. A., Harder, D., Poppe, B., and Chofor, N. (2015). "Water equivalent phantom materials for ^{192}Ir brachytherapy," *Phys. Med. Biol*. 60(24), 9403-9420. https://doi.org/10.1088/0031-9155/60/24/9403

Shakhreet, B. Z., Bauk, S., and Shukri, A. (2013). "Mass attenuation coefficients of fabricated *Rhizophora spp*. particleboard for the 15.77–25.27 keV range," *American J Sci. Ind. Res.* 4(1), 89-94. https://doi.org/10.5251/ajsir.2013.4.1.89.94

Tayo, L. T., Nayaka, D. S., Cárdenas-Oscanoa, A. J., and Euring, M. (2025). "Enhancing physical and mechanical properties of single-layer particleboards bonded with canola protein adhesives: Impact of production parameters," *Eur. J. Wood Wood Prod.* 83(6), 1-18. https://doi.org/10.1007/s00107-024-02163-2

Watanabe, Y., and Constantinou, C. (2006). "Phantom materials in radiology," in: *Encyclopedia of Medical Devices and Instrumentation*, John G. Webster (ed.), second Ed., John Wiley & Sons, Inc., NJ, USA, pp. 252-269. https://doi.org/10.1002/0471732877.emd201

Wibowo, E. S., and Park, B. D. (2021). "Direct measurement of surface adhesion between thin films of nanocellulose and urea-formaldehyde resin adhesives," *Cellulose* 28(13), 8459-8481. https://doi.org/10.1007/s10570-021-04088-y

Xian-qing, X., Ying-ying, Y., Yi-ting, N., and Liang-ting, Z. (2020). "Development of a cornstarch adhesive for laminated veneer lumber bonding for use in engineered wood flooring," *Int. J. Adhes. Adhes.* 98, article 102534. https://doi.org/10.1016/j.ijadhadh.2019.102534

Xu, R., Huang, J., Xu, S., Cai, S., and Liu, W. (2024). "A straw-soy protein composite (SSPC) material: Preparation, physical properties, and wetting drying stability," *Low-carbon Mater. Green Constr.* 2(15), 1-11. https://doi.org/10.1007/s44242-024-00046-6

Younesi-Kordkheili, H., and Pizzi, A. (2026). "Plywood bio-adhesives by oxidized lignin urea bridged with oxidized starch," *J Renew Mater.* 14(1), 1-15. https://doi.org/10.32604/jrm.2025.02025-0179

Zou, Q., Zheng, Y., Liu, Y., Luo, L., Chen, Y., Ran, G., and Liu, D. (2024). "Preparation of cassia bean gum/soy protein isolate composite matrix emulsion gel and its effect on the stability of meat sausage," *Gels* 10(10), article 643. https://doi.org/10.3390/gels10100643

Zuber, S. H., Hadi, M. F. R. A., Hashikin, N. A. A., Yusof, M. F. M., Aziz, M. Z. A., Hashim, R., Samson, D. O., and Isa, N. M. (2022). "Estimation of linear and mass attenuation coefficients of soy-lignin bonded *Rhizophora spp*. particleboard as a potential phantom material using caesium-137 and cobalt-60," *Radiat. Environ. Biophys.* 61, 435-443. https://doi.org/10.1007/s00411-022-00978-2

Zuber, S. H., Hadi, M. F. R. A., Hashikin, N. A. A., Samson, D. O., Ishak, N. H., Raof, N. A., Aziz, M. Z. A., Yusof, M. F. M., and Rabaiee, N. A. (2025). "Dosimetric evaluation of brain radiotherapy using custom-made *Rhizophora* head phantom-comparison between Monte Carlo GATE and treatment planning system MONACO," *Int. J. Radiat. Res.* 23(1), 13-20. https://doi.org/10.61186/ijrr.23.1.13

Article submitted: April 21, 2026; Peer review completed: June 7, 2026; Revised version received and accepted: June 22, 2026; Published: July 7, 2026.
DOI: 10.15376/biores.21.3.7769-7789